Journal of Materials Research and Technology 33 (2024) 2764–2772

Contents lists available at ScienceDirect

Journal of Materials Research and Technology

journal homepage: www.elsevier.com/locate/jmrt

The impact of heat treatment process on the drilling characteristics of Al–5Si–1Cu–Mg alloy produced by sand casting

Şenol Bayraktar [a,*], Cem Alparslan [a], Nurten Salihoğlu [a], Murat Sarıkaya [b,c]

[a] Mechanical Engineering, Recep Tayyip Erdoğan University, Rize, Turkiye
[b] Department of Mechanical Engineering, Sinop University, Turkiye
[c] Faculty of Mechanical Engineering, Opole University of Technology, 45-758, Opole, Poland

ARTICLE INFO

Handling editor: P Rios

Keywords:
Al-5Si–1Cu–Mg alloy
Microstructure
Mechanical properties
Machinability characteristics
Heat treatment

ABSTRACT

Aluminum–Silicon (Al–Si) based materials are commonly preferred in engineering studies requiring high mechanical performance as an alternative to steel materials. These alloys are especially preferred in the automotive industry, aerospace components and heavy machinery parts. In post-casting processes, machining operations are of great importance for high geometric precision, surface quality and longer fatigue life in mechanical environments. In this research, the microstructural, mechanical and machining characteristics of the Al–5Si–1Cu–Mg material produced by sand casting method in both as-cast (AC) and heat-treated (HTed) (Solid solution, quenching and aging-SQA) states were experimentally investigated. Microstructural examinations were carried out with optical microscope and SEM images. Mechanical properties were determined by tensile and hardness tests. Then, drilling experiments were performed in the CNC vertical machining center with 8 mm diameter uncoated HSS (High Speed Steel) cutting tools at constant cutting conditions (i.e., cutting speed-*V*: 125 m/min, feed rate-*f*: 0.05 mm/rev and depth of cut-DoC: 15 mm). In microstructural investigations, it was determined that the microstructure of the Al–5Si–1Cu–Mg material in AC state consists of α-Al, eutectic Si, β-Fe (β-Al_5FeSi) and π-Fe (π-$Al_8Mg_3FeSi_6$) intermetallics. After the SQA, the existing phases generally exhibited a spherical structure, and it was seen that the β phase in the microstructure transformed into the Θ (Al_7FeCu_2) phase. SQA improved the hardness, yield and tensile durability of the material, whereas decreasing the elongation to fracture. SQA process improved the machining characteristics of the material by decreasing thrust force, moment, surface roughness and built-up edge (BUE) formation. The machined subsurface structure of HTed alloy under constant cutting conditions was determined to be more stable and smooth and the machined surface microhardness of HTed alloy was higher compared to as-cast alloy due to the effect of solid precipitation hardening. In addition, shorter and more broken chips occurred in the machining of HTed alloys due to the effect of low elongation to fracture.

1. Introduction

Al–Si materials are frequently preferred in gasoline and diesel engines in the automotive sector in terms of their high specific durability, temperature resistance, thermal conductivity and superior castability properties [1,2]. Diesel engines offer further enhanced power, economy and high thermal efficiency under severe operating conditions. This situation reveals the need to develop the mechanical features of Al–Si-based materials. On the other hand, an important factor limiting the use of Al–Si-based materials is their poor toughness under load. This occurs largely due to the plate-like irregular morphology of the brittle eutectic Si phases [3]. By adding different elements to Al–Si alloys, their mechanical and physical properties can be improved. While Si improves the castability, fluidity and mechanical features of aluminum materials, the copper and magnesium addition increases the strength and hardness features [4]. The addition of Cu increases the hardening and aging potential of the alloy, providing strength at high temperatures. Mg, on the other hand, increases mechanical strength and improves corrosion resistance by promoting precipitation hardening [5,6]. Mg addition increases the strength of the material during aging by precipitating submicroscopic and metastable structures including Mg and Si. These phases ensure excellent barriers to dislocation motion [7,8]. The

* Corresponding author.
E-mail address: senol.bayraktar@erdogan.edu.tr (Ş. Bayraktar).

https://doi.org/10.1016/j.jmrt.2024.10.010
Received 31 July 2024; Received in revised form 28 September 2024; Accepted 2 October 2024
Available online 4 October 2024
2238-7854/© 2024 The Authors. Published by Elsevier B.V. This is an open access article under the CC BY-NC-ND license (http://creativecommons.org/licenses/by-nc-nd/4.0/).

addition of up to 0.5% Mg by weight in Al–Si materials causes the creation of a Mg_2Si structure in the form of point, round, black spalls at the edges of eutectic Si spalls. This allows a significant modification of the eutectic Si phase and the transformation of a large part of the β-Al_5FeSi iron (Fe)-containing intermetallic into a Chinese alphabet-like structure with a composition close to the $Al_8Mg_3FeSi_6$ phase [9]. Mg significantly impacts the type and total volume fraction of Fe-containing structures, especially in materials that do not contain beryllium (Be). In low-Mg content alloys, Fe-rich intermetallic phases consist almost entirely of small β-Al_5FeSi plates. In alloys containing high Mg, large π-Al8Mg3-FeSi6 particles become dominant with a small ratio of β phase [10]. Moreover, the solidification rate has a significant impact on the shape, size and distribution of microstructural. This variable causes Al dendrites to differ in size and composition of eutectic Si and pore size, as well as Fe intermetallics. In Al–Si–Cu materials, the existence of Cu causes the formation of the $CuAl_2$ phase. It was observed that this block-like $CuAl_2$ phase did not dissolve during HT [11]. When brittle $CuAl_2$ is present, the fracture mechanism cannot be controlled by eutectic Si particles. In addition, the impact features of Al–Si casting materials containing Cu are poor, and the existence of Cu greatly contributes to the reduction of impact features. The fracture characteristic of the alloy is affected by undissolved Cu structures, not by Si particles. If Fe is present in the material, platelet-shaped β-Al_5FeSi and code-like α-Al_{15} $(Mn,Fe)_3Si_2$ intermetallics are formed during solidification. During the solidification, β-Al_5FeSi platelets serve as active areas for the nucleation of the $CuAl_2$. Since the solubility of Fe in the Al matrix is negligible, Fe intermetallics are less likely to dissolve completely; however, a certain amount of fragmentation and globalization may reveal [12].

In Al–Si–Cu–Mg alloys, hardness and tensile strength features decrease due to the transformation of precipitates in the microstructure into a coarser-grained structure under the influence of working conditions at temperatures higher than 200 °C in repetitive cyclic loading in mechanical systems. The coexistence of Cu and Mg in these alloys significantly improves the heat treatment ability. Heat treatment is widely applied to improve the mechanical features of aluminium materials [13,14]. T6 heat treatment (HT) is one of the most frequently preferred methods in this context and consists of solution and artificial aging stages. This process changes the microstructure of the alloy and increases its properties such as strength, hardness and durability [15, 16]. Solution HT of Al–Si–Cu–Mg materials is applied to homogenize the material, improve the morphology of interdendritic structures, and dissolve hardening precipitation phases such as $CuAl_2$, Al_2MgCu and Mg_2Si [17]. This process optimizes the solubility and distribution of many phases in the alloy, providing a decisive effect on the mechanical properties.

Components produced by casting for industrial applications must be subjected to machining operations before use to work efficiently in mechanical systems. This is an important process to achieve maximum efficiency in terms of dimensional stability, surface quality, service and fatigue life. In machining operations, input factors such as *V*, *f*, DoC, coolant, cutting tool material and coating are decisive on quality characteristics. This situation requires a more comprehensive investigation of the machining properties of these materials. Bolt or pin joining methods can be preferred in the assembly of automotive equipment such as engine blocks, cylinder heads, pistons and rims made of Al–Si based alloys. For this purpose, it is extremely important to apply drilling operations to these materials to ensure optimum dimensional and geometric tolerance stability after casting. Some research in the academic community on the machining properties of Al–Si based materials are as follows: Machado et al. [18] reported that T6 heat treatment of Al-(% 3–12)Si-0.6 Mg materials (10 h of solution at 540 °C, quenching at 25 °C, and 5 h of artificial aging at 155 °C) increased the hardness of the alloy by approximately 1.6 times compared to the as-cast state. Moreover, the increase in hardness also improved the machinability characteristics. Bayraktar and Hekimoğlu [19] while turning Al–12Si-0.1Sr alloy (Uncoated carbide insert, *V*: 200, 300 and 400 m/min, *f*: 0.05; 0.1 and 0.15 mm/rev, DoC: 1.5 mm) found that cutting force-*F*, surface roughness-*Ra* and BUE formation reduced with rising cutting speed, whereas they increased with rising feed rate. Gonçalves et al. [20] studied the effect of Cu content (0.07–1.93%) and feed on machining properties in drilling Al–Si–Mg (AA6351) alloy (*V*: 60–100 m/min and *f*: 0.1–0.3 mm/rev). They stated that torque and feed forces increased, and the machined surface quality decreased at feed rates higher than 0.2 mm/rev in alloys containing 1.43% and 1.93% Cu. Barakat et al. [21] investigated the machining features of Al–Si based A319 and A356 and Al–Cu alloys in drilling and tapping processes. It was reported that the highest cutting force (approximately 360 N) in T6 HTed Al–Si based alloys was measured after 2500 holes. Moreover, it was found that high Cu content in Al–Cu based alloys reduces tool wear by acting as a lubricant (Approximately 2700 holes). Sadiq et al. [22] found that surface roughness decreased as the speed increased in drilling AA6061T6, LM6 and AA5083 alloys. Additionally, they observed that while minimal BUE was formed under constant cutting conditions in AA6061T6 and AA5083 alloys, relatively more BUE was formed in the LM6 material. Bayraktar and Demir [23] turned the AC and T6 HTed Al–12Si-0.6 Mg material produced by the permanent mold casting technique and found that the minimum *Ra*, *F*, BUE and built-up layer (BUL) were achieved with uncoated tools and that the HT improved the machining properties of the material. Giasin et al. [24] found that the *Ra*, burr height and thickness increased with increasing *f* when drilling Al2024-T3 alloy.

When the literature is generally evaluated, it is seen that the structural, mechanical and machining (SMM) characteristics of Al–Si based materials have been studied in a limited way. Moreover, it has been revealed that the SMM features of the Al–5Si–1Cu–Mg material, which is exposed to repeated thermal cyclic processes, in the AC and HTed state have not been researched. In this research, it was aimed to investigate the structural and mechanical properties of the AC and HTed Al–5Si–1Cu–Mg material produced by sand casting method, as well as the thrust force, moment, surface roughness, machined subsurface hardness and tool wear in the drilling process. Therefore, it is intended to contribute to the academic and industrial sectors by optimizing the production and processing parameters of cast components.

2. Experimental procedure

In the study, sand-cast and heat-treated samples were prepared in appropriate dimensions and geometry for microstructural, mechanical and processing tests. Microstructural examinations were carried out with optical microscope and SEM. Hardness and tensile tests were applied for mechanical examinations. Outputs such as feed force, moment, surface roughness, machined subsurface hardness, BUE and BUL were analyzed for machinability tests in the drilling process. The workflow diagram for the procedure is given in Fig. 1.

2.1. Preparation of sand casted specimens

In this study, the quaternary Al–5Si–1Cu–Mg alloy consisting of Al, Si, Cu and Mg elements was manufactured by sand mold casting technique. Commercial purity aluminum (99.7%), Si, Cu and Mg elements were used to produce the alloy. The elemental composition of the material (wt.%) was specified by analysis with the ICP-OES technique and results are tabulated in Table 1.

The components forming the alloy were melted at a temperature range of 700 ± 5 °C. This molten structure was poured into a pre-prepared sand mold with an angled prismatic mold cavity, allowing the alloys to solidify at room temperature. After the solidification process was completed, the sand mold was dismantled and cast samples were obtained. A total of eight of these samples were produced and prepared for microstructure, mechanical and processability tests in AC and HTed conditions. Before the tests, the cast materials were adjusted to the dimensions with a pre-machining operation on the universal

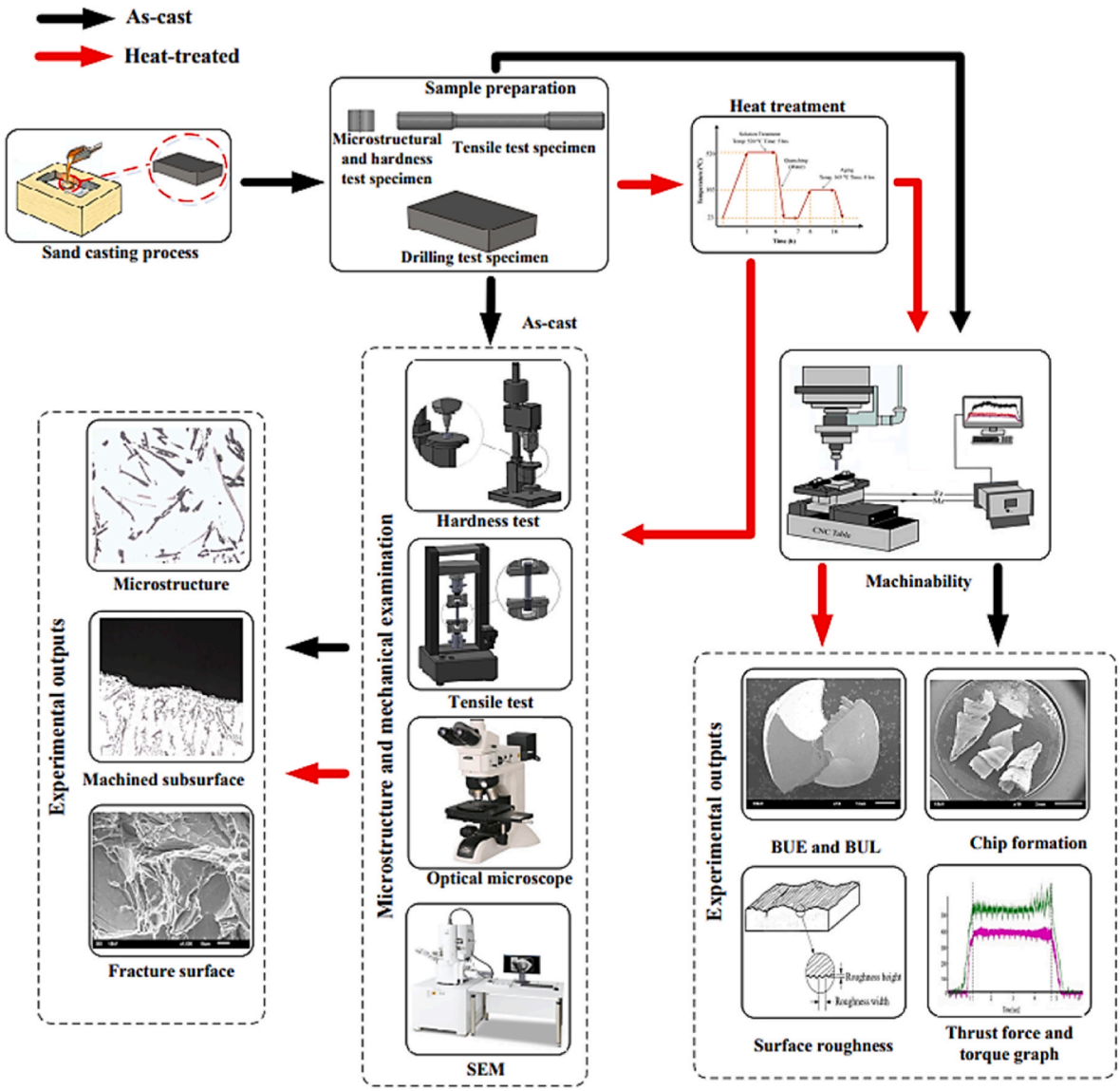

Fig. 1. Workflow diagram.

Table 1
The composition of Al–5Si–1Cu–Mg alloy.

Alloy		Element (wt.%)								
		Si	Fe	Cu	Mn	Mg	Ni	Zn	Ti	Al
Al–5Si–1Cu–Mg	min	4.5	<0.01	1.10	<0.01	0.45	<0.01	<0.01	<0.01	Balance
	max	5.5	0.5	1.50	0.1	0.65	0.10	0.05	0.15	

milling machine and were prepared for drilling tests in the CNC Johnford VMC-850 milling machine (7.5 kW). The samples were then subjected to solid solution processes at 520 °C for 5 h and quenching at 60 °C water temperature for 25 min and then aging at 165 °C for 8 h was applied in a Protherm Mos 170/8 model oven [25,26].

2.2. Preparation of microstructural, hardness, tensile and drilling test samples

The microstructure sample taken from the workpiece produced by sand casting method in as-cast and heat-treated condition was placed in bakelite by mixing powder and hardening liquid in the ratio of 2/1. Sanding, polishing and etching processes were applied to the samples removed from the bakelite container, respectively. After these procedures, the samples were made ready for microstructural examinations. Microstructural examinations were performed using OM and SEM. Phase analysis of the internal structure of the alloy was carried out using energy dispersive spectroscopy (EDS).

In order to determine the mechanical features of the material, AC and HTed samples were prepared for hardness and tensile tests (Fig. 2). Hardnesses were specified on a Qness Q250CS brand equipment using a 62.5 kgf load and a 2.5 mm diameter tip based on Brinell hardness method. Measurement processes were repeated five times for each of the AC and HTed pieces and the final hardness values were specified by calculating the averages. Tensile tests were performed using a constant jaw speed of 0.25 mm/min and an average deformation rate of 5.9 × 10-

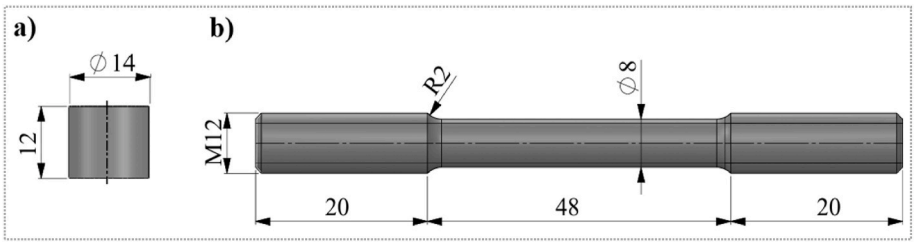

Fig. 2. Manufactured of samples for mechanical examinations, (a) Hardness sample and (b) Tensile sample.

3s-1. A total of six tensile tests were carried out using three samples for each of the AC and HTed samples. Elongation to fracture, yield and tensile strength were determined by calculating the mean of the obtained measurement values. The fracture surfaces formed as a result of tensile tests were imaged with SEM.

Drilling tests on AC and HTed alloys were performed with uncoated HSS drills (Diameter: 8 mm, point angle: 118°, cutting length: 75 mm and standard number: DIN338). At the end of the preliminary drilling experiments, the final cutting parameters (i.e., *V*: 125 m/min, *f*: 0.05 mm/rev and DoC:15 mm) were determined. The vibration signals obtained with the dynamometer during the drilling process were transmitted to the Kistler 5070A amplifier and these vibration signals were transferred to the graphics with the data reading card and Dynoware software. As a result of each experiment, thrust force (Fz) and moment (Mz) values were determined through these graphs in the Dynoware software as seen in Fig. 3.

Mahr Perthometer M1 brand equipment was used to state the average *Ra* in the holes, taking into account the ISO 4287 standard. During measurement, the sampling length was taken as 0.8 mm and the measurement length was 5.6 mm. Four measurements were taken at 90° angles from the entrance, middle and exit points of each machined hole. The final average surface roughness values (Ra-μm) were obtained by taking the arithmetic average of these measurements. After the drilling process, subsurface hardness measurements were carried out on the sample. After these samples were cut, they were sanded using bakelite and then subjected to polishing processes. Vickers micro hardness tests were applied to the polished machined surfaces at a load of 4.90 N/50 g and an immersion time of 10 s. During the tests, measurements were taken at 10 μm intervals, starting from just below the machined surface, and microhardness values were determined.

3. Results and discussion

3.1. Microstructural and mechanical observations

Optical microscope images of the microstructures of AC and HTed Al–5Si–1Cu–Mg materials are shown in Fig. 4. It has been observed that the internal structure of the as-cast alloys consists of rich-aluminum α, fibrous eutectic Si, acicular β-Al_5FeSi and π-Fe ($Al_8Mg_3FeSi_6$). With the effect of 0.35% Mg content, the β-Al_5FeSi phase in the structure of the alloy turned into the π-Fe phase [27]. It was observed that with the dissolution and aging process applied to the alloy (T6 heat treatment), the Si particles in the internal structure became spherical with the impact of the precipitate hardening property and exhibited a grained structure of smaller sizes as seen in Fig. 5. Additionally, it was determined that the intermetallic β-Al_5FeSi phase precipitated and transformed into Θ (Al_7FeCu_2) phase due to heat treatment [28,29]. It is thought that the spheroidization of Si particles and the formation of Al_7FeCu_2 intermetallic phase reduces the elongation to fracture by increasing the hardness, yield and tensile strength of the material. The chemical compositions of the phases in the microstructure of the Al–5Si–1Cu–Mg alloy are presented in Table 2. The obtained results support the findings in the literature [30].

Hardness, elongation to fracture, yield and tensile strength of AC and

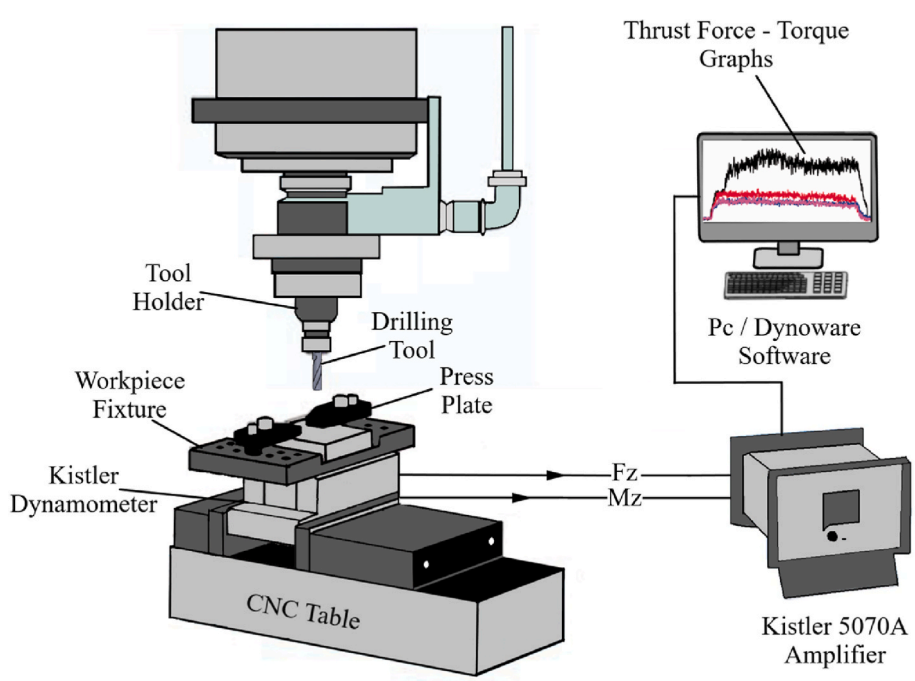

Fig. 3. Drilling experiment setup.

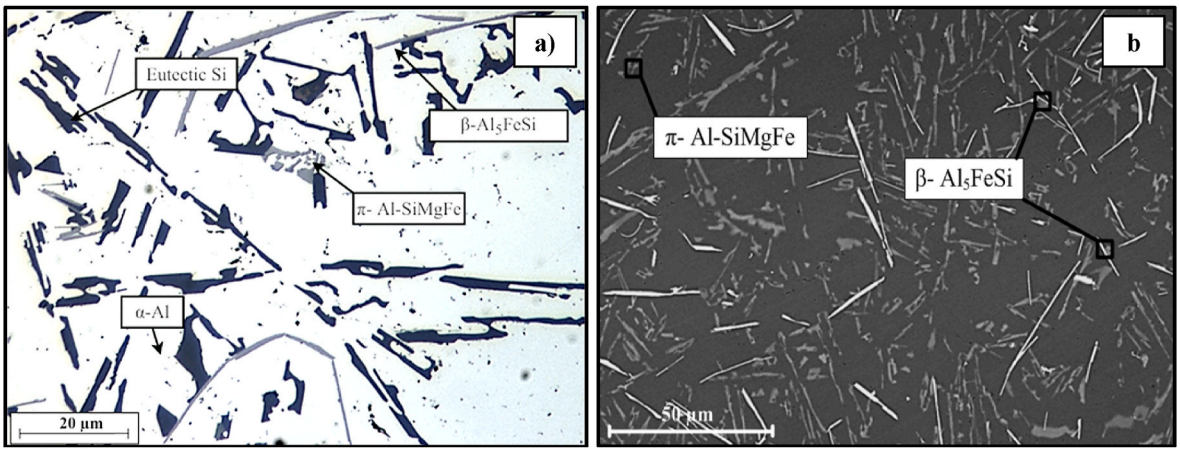

Fig. 4. Representation of the microstructure of Al–5Si–1Cu–Mg material in the AC state, (a) Optic microscope and, (b) SEM images.

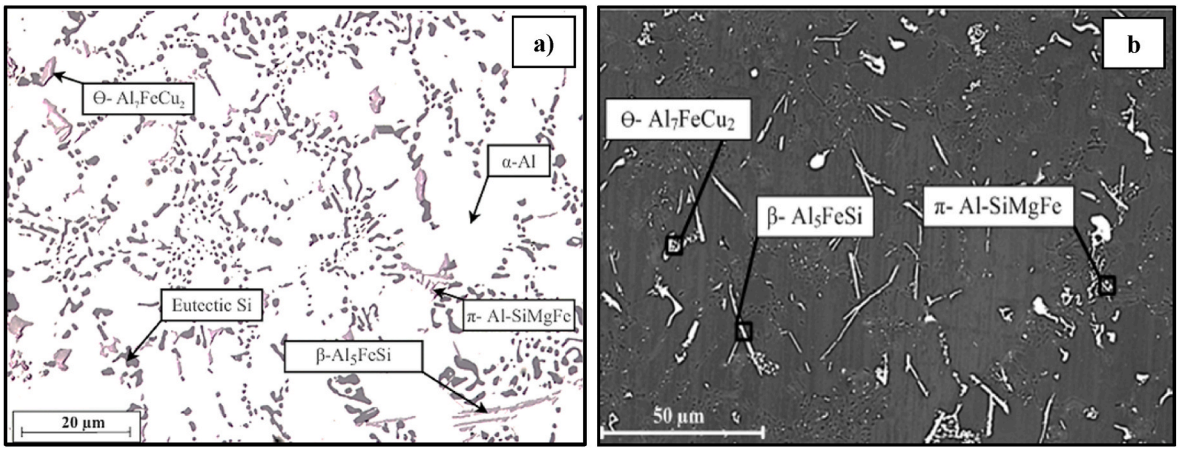

Fig. 5. Representation of the microstructure of Al–5Si–1Cu–Mg alloy in the HTed state, (a) OM and, (b) SEM images.

Table 2
Semi-quantitative compositions of phases.

Chemical composition (wt.%)						
Phase	Al	Si	Fe	Cu	Mg	Mn
β-Al_5FeSi (Observed)	58.0–70.0	12.3–17.7	15.6–22.5	0.1–0.3	–	–
β-Al_5FeSi (In literature) [30]	45.2–75.8	5.2–15.0	17.9–35.0	–	–	–
π (Observed)	57.4–87.1	7.8–23.3	2.2–15.0	1.4–5.5	2.3–7.5	0.4–1.9
π (In literature) [30]	37.7–54.0	25.0–33.8	0.8–11.5	5.3–12.5	9.0–16.0	–
θ (observed)	50.3–70.0	0.7–1.2	0.9–3.5	20–38.5	–	–
θ (literature) [30]	47.5–55.0	–	–	49.5–52.5	–	–

HTed materials are shown in Table 3. It was determined that after HT, hardness, yield and tensile durability of the material increased by 29.41%, 28.57% and 44.11%, respectively, while the elongation to fracture decreased by 38.88%. It is thought that solid solution hardening after HT increases hardness, yield and tensile durability values [31] and reduces elongation to fracture [16,32]. In Al–Si based materials, HT, apart from spheroidization, thins the eutectic Si particles and distributes them homogeneously within the microstructure. With homogeneously distributed particles, the resistance to nucleation and crack growth in the microstructure of alloys increases. Therefore, it is thought that the stress required for the formation of a void or crack at the particle/matrix interface in the microstructure increases with the spherical morphology that occurs due to heat treatment [33]. Solid solution and aging processes change the morphology of the eutectic Si phase at grain boundaries due to recrystallization. In addition, it causes the dissolution of intermetallic compounds in the α-Al matrix and the formation of a

Table 3
Tensile strength, yield strength, hardness and elongation to fracture values of AC and T6 (SQA) HTed alloys.

Alloy	Tensile strength (N/mm^2)	Yield strength (N/mm^2)	Hardness of Brinell (HB)	Elongation to fracture (%)
As-cast	170	140	85	1.8
Heat treated	245	180	110	1.1

spherical eutectic Si phase at grain boundaries. In other words, the aim of rearranging grain boundaries is to obtain more regular and spherical particles.

SEM images of the fracture surfaces resulting from the tensile tests of the AC and HTed alloy are given in Fig. 6. It was determined that there were pits, ridges, cleavage planes and microcracks in the fracture surface images. It is thought that the fracture occurs by following the dendrite boundaries and intermetallic phases as well as Si particles have a significant effect on the fracture characteristics. It has been determined that alloys exhibit transgranular brittle fracture characteristics due to the decrease in elongation to fracture with heat treatment [23,34]. This fracture behavior can be associated with the distribution of Si and other secondary phases in the microstructure of the material and the bonding characteristics with the matrix.

Under the stress applied to the alloy, large Fe-rich intermetallic phases can accumulate at the interface between the intermetallic particle and the α-Al matrix, preventing dislocation movement. This situation triggers stress concentration that supports particle cracking and crack nucleation [35]. Irregular structures, large pits and obvious microcracks were observed on the fracture surface of the AC Al–5Si–1Cu–Mg alloy (Fig. 6a). The fracture mechanism in the as-cast alloy is characterized by large pits and intermetallic phase compounds that facilitate the formation of larger secondary cracks. Internal stresses resulting from plastic deformation occur during fracture [36]. As a result of these internal stresses, the fracture path develops along interdendritic regions characterized by high-density Fe-rich intermetallic phases, where the damage process begins with particle cracking [27]. The increase in Si particle size and aspect ratio causes higher stress. The probability of fracture increases as a result of high stress. Brittle particle groups provide both high particle cracking rate and microcracks bonding during damage. This situation has been shown in previous studies that Fe-based intermetallics (Figs. 4 and 5), which are present in a large volume fraction, have a significant effect on the fracture of alloys [27]. After T6 heat treatment, most of the particles in the internal structure dissolve in the α-Al matrix phase. This reduces the impact on energy caused by the brittle structure of the particles. Due to the fibrous structure of the spheroidized particles (refer to Fig. 5a) during HT, the disintegration of intermetallic phases containing Fe reduces the possibility of crack formation along these particles [26].

3.2. Machinability characteristics of sand casted alloy

As shown in Fig. 7, thrust force (Fz), Ra and moment (Mz) values were determined when drilling AC and HTed alloys on a vertical machining center under constant *V*, *f* and DoC conditions. As a result of the solid solution and aging process, it was stated that the *Ra*, thrust force and moment values decreased by 25.99%, 11.31% and 11.63%,

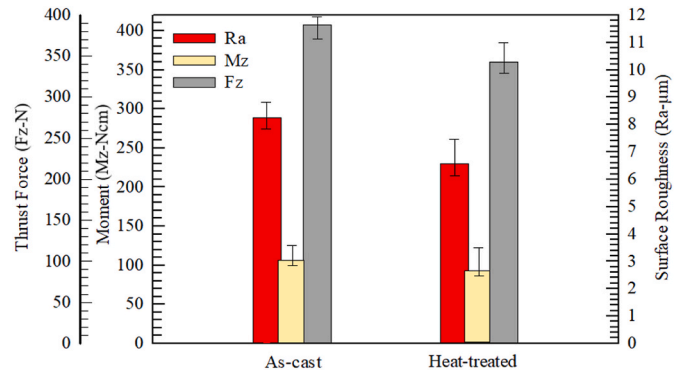

Fig. 7. Fz, Mz and Ra relationship in machining of alloys.

respectively. The phases in the microstructure play an important role on the machinability characteristics of alloys. After HT, these phases are called soluble and insoluble. Soluble phases consist of elements that dissolve in the α-Al matrix with the effect of HT and are located as soft particles. The other is called phases that cannot be dissolved by HT. Insoluble phases contain high amounts of Fe and contain harder and brittle particles compared to soluble phases. These particles have the potential to wear the cutting tool [37]. On the other hand, these particles can increase the formation of BUE in the cutting edge by sweeping the ductile α-Al phase. Heat treatment applied to Al–Si based materials in manufacturing is an important factor to improve the machining properties in machining operations. At the same time, the hardness of the material is among the metallurgical variables in controlling the machining properties [23]. Unlike many other metals, these alloys generally improve their machinability as hardness increases. The vast majority of businesses in the automotive sector accept that a minimum hardness of 80 Brinell is a desirable value [38]. Precipitate hardening occurs in the dissolved phases due to the effect of HT during machining experiments. This situation facilitates fracture during drilling, accelerates the evacuation of the chip from the cutting zone and is thought to reduce thrust force and torque. With the easy evacuation of the chip, the scratch marks and surface roughness on the machined hole surface are minimized. After the drilling process, the microhardness of the machined surface and subsurface was determined as presented in Fig. 8. Here, a measurement range of 10–140 µm was used for distance from cutting edge. In the measurements, it was demonstrated that the microhardness values of heat-treated samples were relatively higher than as-cast samples. This is associated with the high macro hardness value due to the hardening of the solid precipitate formed in the microstructure by heat treatment [31,39]. It is thought that the grain size in the microstructure decreases due to the effect of heat resulting

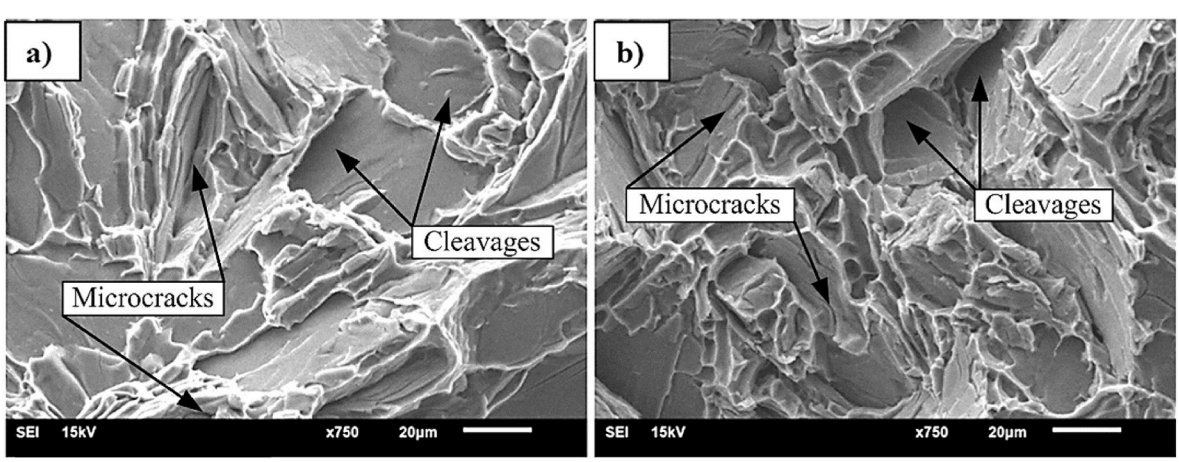

Fig. 6. SEM photographs for fracture surface (a) AC and (b) HTed.

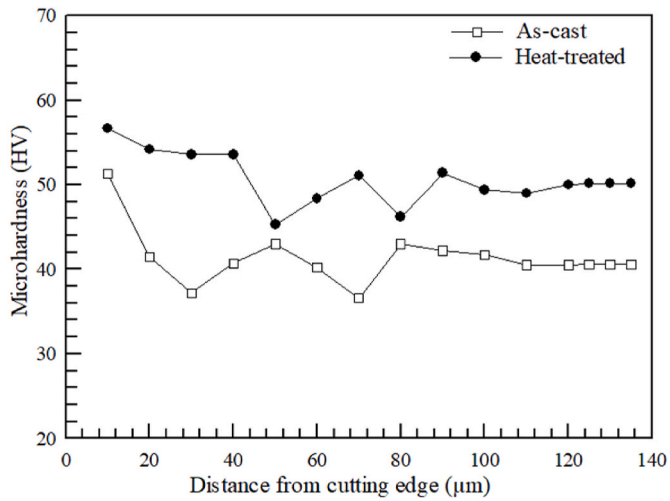

Fig. 8. Microhardness values for machined subsurface of Al–5Si–1Cu–Mg alloy.

from deformation and friction at the tool-workpiece interface during cutting and, accordingly, the microhardness value on the machined surface increases. In general, it is known that high cutting temperature caused by the interaction between the cutting edge and the newly machined surface causes differences in microhardness values, which contributes to plastic deformation on the free surface of the workpiece [40].

At the end of the drilling process, subsurface images of the machined surface based on drilling direction in AC and HTed alloys are given in Fig. 9. In these images, Si particles are in contact with the cutting tool due to the friction between the cutting tool and the workpiece during machining. As a result of this contact, Si particles in the microstructure can be broken and sprinkled on the machined surface (fallout). As seen in Fig. 9, the fractures are quite obvious, and it is thought that the voids formed in the treated subsurface are caused by the dislocation of broken particles together with the ductile α-Al matrix phase. This can cause an increase in *Ra* [40]. It is seen that the treated subsurface structure of the heat-treated alloy is more stable and smoother than the as-cast alloy (Fig. 9b). This situation is thought to be due to the decrease in the elongation to fracture of the alloy with HT and the easy breakage of the chip. In other words, the alloy turns into a more brittle structure and fracture occurs more easily. Fracture may occur more easily and defects that may arise from the hard Si phase on the machined surface may occur less frequently than in the as-cast alloy.

The SEM image of the drills used in the drilling of alloys is shown in Fig. 10. It was observed that BUE formation in the cutting tool decreased in the drilling of heat-treated alloys (Fig. 10b). Low hardness and high ductility in Al-based alloys trigger BUE formation on the cutting edge. Heat treatment applied to the alloy increases the hardness of the material, reduces BUE in the cutting tool and can improve the machined surface quality [38]. In other words, the decrease in elongation to fracture due to heat treatment facilitates chip breaking and evacuation from the cutting zone. This improves the machined surface quality by reducing BUE, cutting force and surface roughness (refer to Fig. 7) [41, 42]. During cutting, BUL initially occurs with the extrusion of the ductile α-Al with a low melting point on the rake face of the cutting tool. As the cutting process continues, the elements with a high melting point (Al–Si–Cu–Mg residues) in the alloy are swept away by the impact of friction and compression forces (refer to Fig. 10-Spectrum A and B). This situation causes the transformation of BUL amount to BUE at the cutting edge. As a result of the welding of BUE to the cutting edge, the tool geometry is disrupted by breaking off the particles from the tool material during cutting. Disrupted tool geometry is an important phenomenon that increases the cutting force and surface roughness.

In the drilling of as-cast alloy, chip morphology was observed to be longer and more curved than heat-treated alloy (Fig. 11 (a)). It is thought that the low elongation to fracture measured in heat-treated alloy contributes to the formation of shorter and more broken chip (Fig. 11 (b)) by facilitating chip breakage during cutting compared to as-cast alloy [23]. Short and broken chip formation can be considered as a result of brittle fracture characteristics. Short chip formation is a desired event for ideal surface quality and occupational safety in machining operations.

4. Conclusions

In this study, SMM features of AC and HTed Al–Si–Cu–Mg alloys were comparatively investigated. Microstructural analyses showed that the alloy in the AC condition consisted of α-Al, eutectic Si and many plate and acicular β-Fe (β-Al_5FeSi) and script-like π-Fe (π-$Al_8Mg_3FeSi_6$) intermetallics rich in Fe. It was determined that these phases partially dissolved and aggregated with heat treatment, became spherical and that the β phase transformed into Θ (Al_7FeCu_2) phase after aging. Mechanical tests revealed that heat treatment increased the hardness, yield and tensile durability of the material, whereas decreasing the elongation to fracture. In addition, it was determined that the fracture surfaces exhibited transgranular brittle fracture characteristics with heat treatment after the tensile test. In terms of machinability, it was found that the thrust force, moment, *Ra* and BUE formation reduced with HT and the machined subsurface microhardness values increased up to a certain depth. These findings indicate that HT significantly improves the performance, strength and machining features of Al–5Si–1Cu–Mg materials and increases the potential of these alloys in the automotive and

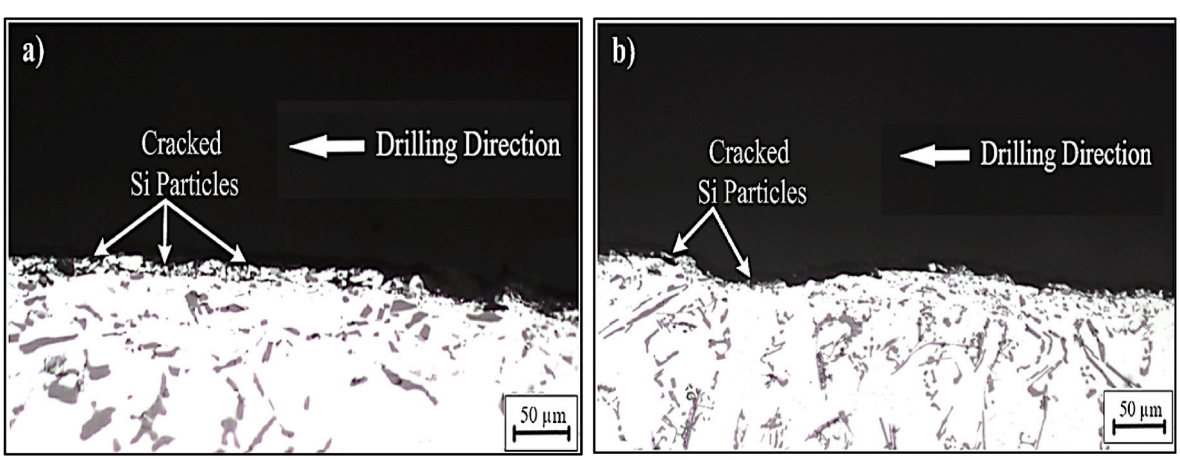

Fig. 9. Machined subsurface images in drilling of alloys, (a) AC alloy and (b) HTed material.

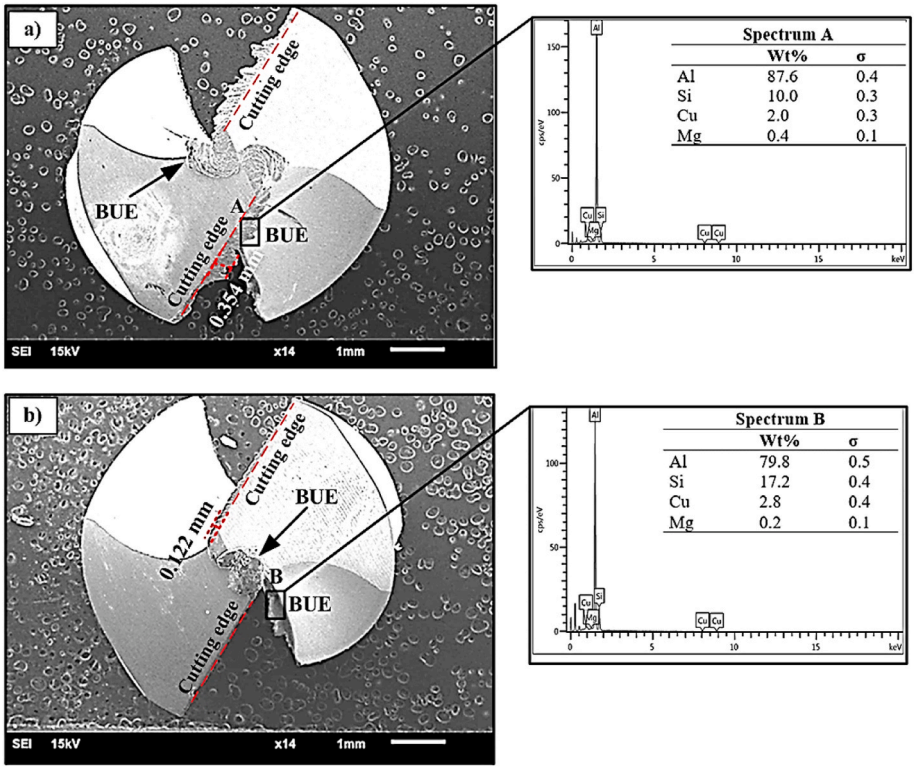

Fig. 10. SEM and EDS images of cutting tools used in drilling alloys, (a) AC alloy and (b) HTed material.

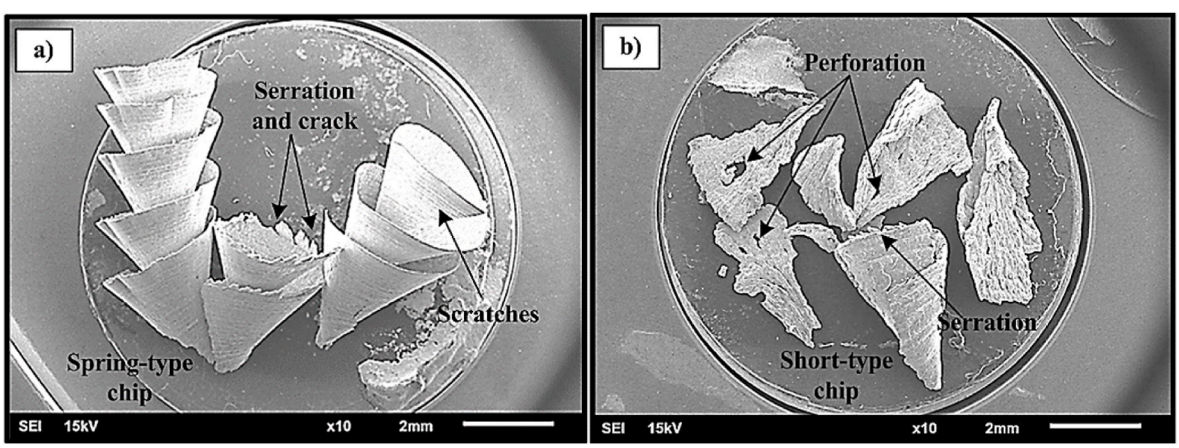

Fig. 11. SEM images of the chips for machined alloys, (a) AC alloy and (b) HTed material.

aerospace sectors.

CRediT authorship contribution statement

Şenol Bayraktar: Supervision, Conceptualization, Methodology, Investigation, Writing – original draft, Writing – review & editing. **Cem Alparslan:** Investigation, Visualization, Software. **Nurten Salihoğlu:** Investigation, Methodology, Visualization. **Murat Sarıkaya:** Methodology, Conceptualization, Writing – review & editing, Validation.

Declaration of competing interest

The authors declare that they have no known competing financial interests or personal relationships that could have appeared to influence the work reported in this paper.

Acknowledgements

The authors would like to thank TÜBİTAK for their support with Project No: 221M064. Additionally, this study has been supported by the Recep Tayyip Erdoğan University Development Foundation (Grant number: 02024008019032).

Murat Sarıkaya acknowledges the Polish National Agency for Academic Exchange (NAWA) under the Ulam Programme (Grant No. BPN/ULM/2023/1/00035).

References

[1] Su B, Chao H, Jin Y, Cui G, Zhong M, Wang B, et al. Influence of heat treatment on microstructure and thermo-physical properties of Al-50wt%Si alloy fabricated by selective laser melting. J Mater Res Technol 2024;30:4542–51. https://doi.org/10.1016/j.jmrt.2024.04.171.

[2] Liu D, Fang Y, Nolte S, Lippmann S. Dendritic Si growth morphologies in highly undercooled Al–Si alloys. J Mater Res Technol 2024;31:520–8. https://doi.org/10.1016/j.jmrt.2024.05.252.
[3] Gall K, Yang N, Horstemeyer M, McDowell DL, Fan J. The debonding and fracture of Si particles during the fatigue of a cast Al-Si alloy. Metall Mater Trans 1999;30:3079–88. https://doi.org/10.1007/s11661-999-0218-2.
[4] Zolotorevsky VS, Belov NA, Glazoff MV. Casting aluminum alloys, vol. 12. Amsterdam: Elsevier; 2007.
[5] Li Z, Samuel AM, Samuel FH, Ravindran C, Valtierra S. Effect of alloying elements on the segregation and dissolution of CuAl2 phase in Al-Si-Cu 319 alloys. J Mater Sci 2003;38:1203–18. https://doi.org/10.1023/A:1022857703995.
[6] Mohamed AMA, Samuel AM, Samuel FH, Doty HW. Influence of additives on the microstructure and tensile properties of near-eutectic Al–10.8%Si cast alloy. Mater Des 2009;30:3943–57. https://doi.org/10.1016/j.matdes.2009.05.042.
[7] Yang H, Ji S, Yang W, Wang Y, Fan Z. Effect of Mg level on the microstructure and mechanical properties of die-cast Al–Si–Cu alloys. Mater Sci Eng, A 2015;642:340–50. https://doi.org/10.1016/j.msea.2015.07.008.
[8] Wang QG, Davidson CJ. Solidification and precipitation behaviour of Al-Si-Mg casting alloys. J Mater Sci 2001;36:739–50. https://doi.org/10.1023/A:1004801327556.
[9] Samuel FH, Samuel AM, Ouellet P, Doty HW. Effect of Mg and Sr additions on the formation of intermetallics in Al-6 Wt pct Si-3.5 Wt pct Cu-(0.45) to (0.8) Wt pct Fe 319-type alloys. Metall Mater Trans 1998;29:2871–84. https://doi.org/10.1007/s11661-998-0194-y.
[10] Xu S-L, Jia H-L, Zha M, Zhou X-L, Gao D, Ma P-K, et al. The effect of B and Sb on the corrosion behavior of T6-treated Al–Si–Mg alloys. J Mater Res Technol 2024;30:3611–21. https://doi.org/10.1016/j.jmrt.2024.04.083.
[11] Elsebaie O, Samuel FH, Alkahtani SA, Doty HW. Influence of metallurgical parameters on the impact toughness of near eutectic Al–Si alloys. Int J Metalcast 2016;10:276–88. https://doi.org/10.1007/s40962-016-0039-1.
[12] Elsharkawi EA, Ibrahim MF, Samuel AM, Doty HW, Samuel FH. Understanding the effect of Be addition on the microstructure and tensile properties of Al–Si–Mg cast alloys. Int J Metalcast 2022;16:1777–95. https://doi.org/10.1007/s40962-021-00715-3.
[13] Beroual S, Boumerzoug Z, Paillard P, Borjon-Piron Y. Effects of heat treatment and addition of small amounts of Cu and Mg on the microstructure and mechanical properties of Al-Si-Cu and Al-Si-Mg cast alloys. J Alloys Compd 2019;784:1026–35. https://doi.org/10.1016/j.jallcom.2018.12.365.
[14] Eisaabadi BG, Yeom GY, Tiryakioğlu M, Netto N, Beygi R, Mehrizi MZ, et al. The effect of solution treatment time on the microstructure and ductility of naturally-aged A383 alloy die castings. Mater Sci Eng, A 2018;722:1–7. https://doi.org/10.1016/j.msea.2018.02.103.
[15] Costa TA, Dias M, Gomes LG, Rocha OL, Garcia A. Effect of solution time in T6 heat treatment on microstructure and hardness of a directionally solidified Al–Si–Cu alloy. J Alloys Compd 2016;683:485–94. https://doi.org/10.1016/j.jallcom.2016.05.099.
[16] Zhu M, Jian Z, Yang G, Zhou Y. Effects of T6 heat treatment on the microstructure, tensile properties, and fracture behavior of the modified A356 alloys. Mater Des 2012;36:243–9. https://doi.org/10.1016/j.matdes.2011.11.018.
[17] Beroual S, Boumerzoug Z, Paillard P, Borjon-Piron Y. Effects of heat treatment and addition of small amounts of Cu and Mg on the microstructure and mechanical properties of Al-Si-Cu and Al-Si-Mg cast alloys. J Alloys Compd 2019;784:1026–35. https://doi.org/10.1016/j.jallcom.2018.12.365.
[18] Machado PAB, do Vale Quaresma JM, Garcia A, dos Santos CA. Investigation on machinability in turning of as-cast and T6 heat-treated Al-(3, 7, 12%)Si-0.6%Mg alloys. J Manuf Process 2022;75:514–26. https://doi.org/10.1016/j.jmapro.2022.01.028.
[19] Bayraktar Ş, Hekimoğlu AP. Performance evaluation of different carbide inserts in turning of newly developed Al-12Si-0.1Sr alloy. Mater Werkst 2023;54:120–8. https://doi.org/10.1002/mawe.202200148.
[20] Gonçalves RA, Silva MB da. Influence of copper content on 6351 aluminum alloy machinability. Procedia Manuf 2015;1:683–95. https://doi.org/10.1016/j.promfg.2015.09.014.
[21] Barakat H, Zedan Y, Samuel AM, Doty HW, Valtierra S, Samuel FH. Effect of metallurgical parameters on the drilling and tapping characteristics of aluminum cast alloys. Int J Adv Des Manuf Technol 2019;105:1357–70. https://doi.org/10.1007/s00170-019-04322-9.
[22] Sadiq TO, Hameed BA, Idris J, Olaoye O, Nursyaza S, Samsudin ZH, et al. Effect of different machining parameters on surface roughness of aluminium alloys based on Si and Mg content. J Braz Soc Mech Sci Eng 2019;41:451. https://doi.org/10.1007/s40430-019-1948-8.
[23] Bayraktar Ş, Demir O. Processing of T6 heat-treated Al-12Si-0.6Mg alloy. Mater Manuf Process 2020;35:354–62. https://doi.org/10.1080/10426914.2020.1732412.
[24] Giasin K, Hodzic A, Phadnis V, Ayvar-Soberanis S. Assessment of cutting forces and hole quality in drilling Al2024 aluminium alloy: experimental and finite element study. Int J Adv Des Manuf Technol 2016;87:2041–61. https://doi.org/10.1007/s00170-016-8563-y.
[25] Cai Q, Mendis CL, Wang S, Chang ITH, Fan Z. Effect of heat treatment on microstructure and tensile properties of die-cast Al-Cu-Si-Mg alloys. J Alloys Compd 2021;881:160559. https://doi.org/10.1016/j.jallcom.2021.160559.
[26] Samuel AM, Doty HW, Valtierra S, Samuel FH. Relationship between tensile and impact properties in Al–Si–Cu–Mg cast alloys and their fracture mechanisms. Mater Des 2014;53:938–46. https://doi.org/10.1016/j.matdes.2013.07.021.
[27] Ceschini L, Morri A, Morri A, Toschi S, Johansson S, Seifeddine S. Effect of microstructure and overaging on the tensile behavior at room and elevated temperature of C355-T6 cast aluminum alloy. Mater Des 2015;83:626–34. https://doi.org/10.1016/j.matdes.2015.06.031.
[28] Sjölander E, Seifeddine S. Optimisation of solution treatment of cast Al–Si–Cu alloys. Mater Des 2010;31:S44–9. https://doi.org/10.1016/j.matdes.2009.10.035.
[29] Son H-W, Lee J-Y, Cho Y-H, Jang J, Kim S-B, Lee J-M. Enhanced mechanical properties and homogeneous T5 age-hardening behavior of Al-Si-Cu-Mg casting alloys. J Alloys Compd 2023;960:170982. https://doi.org/10.1016/j.jallcom.2023.170982.
[30] Mrówka-Nowotnik G, Sieniawski J. Microstructure and mechanical properties of C355. 0 cast aluminium alloy. Arch Mater Sci Eng 2011;47(2):85–94.
[31] Sharma R, Anesh Dwivedi DK. Influence of silicon (wt.%) and heat treatment on abrasive wear behaviour of cast Al–Si–Mg alloys. Mater Sci Eng, A 2005;408:274–80. https://doi.org/10.1016/j.msea.2005.08.013.
[32] Alparslan C, Bayraktar Ş. An experimental study on microstructural, mechanical and machinability properties of as-cast and heat-treated Al-7Si-Mg alloy. Silicon 2024;16:3971–85. https://doi.org/10.1007/s12633-024-02968-z.
[33] Dwivedi DK, Sharma R, Kumar A. Influence of silicon content and heat treatment parameters on mechanical properties of cast Al–Si–Mg alloys. Int J Cast Metals Res 2006;19:275–82. https://doi.org/10.1179/136404606X153867.
[34] Alparslan C, Bayraktar Ş. Experimental research and optimization based on response surface methodology on machining characteristics of cast Al-7Si-0.6 Mg alloy: effects of cutting parameters and heat treatment. Measurement 2024;236:115111. https://doi.org/10.1016/j.measurement.2024.115111.
[35] Ceschini L, Morri A, Toschi S, Seifeddine S. Room and high temperature fatigue behaviour of the A354 and C355 (Al–Si–Cu–Mg) alloys: role of microstructure and heat treatment. Mater Sci Eng, A 2016;653:129–38. https://doi.org/10.1016/j.msea.2015.12.015.
[36] Wang QG. Microstructural effects on the tensile and fracture behavior of aluminum casting alloys A356/357. Metall Mater Trans 2003;34:2887–99. https://doi.org/10.1007/s11661-003-0189-7.
[37] Zedan Y, Samuel FH, Samuel AM, Doty HW. Effects of Fe intermetallics on the machinability of heat-treated Al–(7–11)% Si alloys. J Mater Process Technol 2010;210(2):245–57. https://doi.org/10.1016/j.jmatprotec.2009.09.007.
[38] Tash M, Samuel FH, Mucciardi F, Doty HW, Valtierra S. Effect of metallurgical parameters on the machinability of heat-treated 356 and 319 aluminum alloys. Mater Sci Eng, A 2006;434:207–17. https://doi.org/10.1016/j.msea.2006.06.129.
[39] Xi HH, Ming WQ, He Y, Xie P, Xu XD, Zhang Z, et al. Unveiling the fine microstructure of nanoscale composite particles embedded in brittle Si phase in an Al-Si-Cu-Mg alloy. J Alloys Compd 2022;906:164238. https://doi.org/10.1016/j.jallcom.2022.164238.
[40] Farid AA, Sharif S, Idris MH. Surface integrity study of high-speed drilling of Al–Si alloy using HSS drill. Proc Inst Mech Eng B J Eng Manuf 2011;225:1001–7. https://doi.org/10.1177/2041297510393642.
[41] Yücel A, Yıldırım ÇV, Sarıkaya M, Şirin Ş, Kıvak T, Gupta MK, et al. Influence of MoS2 based nanofluid-MQL on tribological and machining characteristics in turning of AA 2024 T3 aluminum alloy. J Mater Res Technol 2021;15:1688–704. https://doi.org/10.1016/j.jmrt.2021.09.007.
[42] Bayraktar Ş, Afyon F. Machinability properties of Al–7Si, Al–7Si–4Zn and Al–7Si–4Zn–3Cu alloys. J Braz Soc Mech Sci Eng 2020;42:187. https://doi.org/10.1007/s40430-020-02281-x.